GSA Data Repository Item 2014177

Magmatic salt melt and vapor: Extreme fluids forming porphyry gold deposits in shallow subvolcanic settings

by Koděra et al.

APPENDIX DR1: Summary of analytical data from laser ablation inductively coupled plasma mass spectrometry (LA-ICP-MS)

Table DR1: Table of microanalyses of fluid inclusions from the Biely Vrch porphyry gold deposit, and reconnaissance data from the Kráľová porphyry gold occurrence (sample KR5).

Sample and assemblage	Qtz type	Total of inclusions	$FeCl_2$ (wt%)	KCl (wt%)	NaCl (wt%)	Cl (ppm)	Fe (ppm)	K (ppm)	Na (ppm)	Mg (ppm)	Pb (ppm)	Ca (ppm)	Mn (ppm))	S* (ppm)	Cu* (ppm)	Au* (ppm)	Ag* (ppm)	Cs (ppm)	Al (ppm)
Vapor inclusions																			
DVE4_140.3 as.1	banded?	2	41.6	38.7	19.7	914000	183000	203000	78000	21000	n.a.	n.a.	n.a.	21400	1460	27.3	165	n.a.	n.a.
DVE4_140.3 as.3	A	1	55.1	33.1	11.8	604000	243000	174000	46000	1000	n.a.	n.a.	n.a.	tr. ph.	tr. ph.	4.5	tr. ph.	n.a.	n.a.
DVE4_188.6 as.1	A	4	51.9	36.6	11.5	574000	229000	192000	45000	n.d.	n.a.	n.a.	n.a.	8700	2230	23.3	330	n.a.	n.a.
DVE4_188.6 as.2	A?	5	53.7	36.9	9.8	456000	237000	193000	39000	5000	n.a.	n.a.	n.a.	10100	1610	8.2	214	n.a.	n.a.
DVE5a_304.2 as.1	A?	2	48.1	27.4	24.6	n.d.	212000	143000	97000	58000	n.a.	n.a.	n.a.	23900	980	22.3	n.a.	n.a.	n.a.
DVE5a_304.2 as.2	A?	3	47.9	32.1	12.8	178000	211000	168000	50000	65000	n.a.	n.a.	n.a.	11200	50	1.8	n.a.	n.a.	n.a.
DVE5a_304.2 as.3	A?	7	36.8	32.2	28.9	449000	162000	169000	114000	16000	n.a.	n.a.	n.a.	10400	120	19.3	117	n.a.	n.a.
DVE5a_304.2 as.4	banded?	4	35.5	32.7	28.8	459000	156000	172000	113000	3000	n.a.	n.a.	n.a.	4800	50	12.6	63	n.a.	n.a.
DVE5a_369.6 as.1	A	16	50.0	30.7	19.0	646000	220000	161000	75000	n.a.	n.a.	n.a.	n.a.	10000	180	6.6	n.a.	n.a.	n.a.
DVE5a_369.6 as.2	A	6	58.1	30.5	13.2	607000	256000	160000	52000	n.a.	n.a.	n.a.	n.a.	10300	1310	3.8	n.a.	n.a.	n.a.
DVE5a_369.6 as.4	A	3	49.9	28.7	20.9	941000	220000	150000	82000	n.a.	n.a.	n.a.	n.a.	13900	280	4.1	n.a.	n.a.	n.a.
DVE5a_540.5 as.1	A or qtz xenolith	4	51.1	29.0	19.5	787000	225000	152000	77000	300	n.a.	n.a.	n.a.	2300	1320	0.3	n.a.	n.a.	n.a.
DVE5a_104.6 as.1	qtz xenolith	6	n.a.	32.9	22.3	584000	n.a.	173000	88000	n.a.	n.a.	n.a.	n.a.	8900	29680	1.6	n.a.	134	n.a.
DVE5a_104.6 as.2	qtz xenolith	1	57.3	28.5	14.3	653000	252000	149000	56000	n.a.	n.a.	n.a.	n.a.	10700	3450	4.6	n.a.	n.a.	n.a.
DVE5a_104.6 as.3	qtz xenolith	3	37.7	23.9	38.8	n.d.	166000	125000	153000	n.a.	n.a.	n.a.	n.a.	63100	3720	19.9	n.a.	n.a.	n.a.
DVE5a_104.6 as.4	qtz xenolith	1	n.a.	24.0	31.3	517000	n.a.	126000	123000	n.d.	n.a.	n.a.	n.a.	12100	28550	2.9	n.a.	n.a.	n.a.
DVE5a_104.6 as.6	qtz xenolith	3	31.7	31.4	23.9	1667000	140000	165000	94000	19000	n.a.	n.a.	n.a.	14600	970	16.6	83	n.a.	n.a.
DVE5a_104.6 as.8	qtz xenolith	1	54.0	16.8	29.2	n.d.	238000	88000	115000	300	n.a.	n.a.	n.a.	11400	280	5.3	40	n.a.	n.a.
DVE5a_104.6 as.9	qtz xenolith	2	47.6	28.8	23.6	319000	210000	151000	93000	n.d.	n.a.	n.a.	n.a.	1200	2460	1.1	65	n.a.	n.a.
DVE5a_104.6 as.10	qtz xenolith	2	41.9	30.6	26.1	643000	185000	160000	103000	n.a.	n.a.	n.a.	n.a.	6100	14120	2.9	n.a.	73	n.a.
KR5 as.1	banded?	2	23.0	35.3	41.7	478000	101000	185000	164000	300	n.a.	n.a.	n.a.	4100	5750	24.8	335	n.a.	n.a.
KR5 as.2	banded?	1	83.3	8.5	8.2	n.d.	367000	44000	32000	n.d.	n.a.	n.a.	n.a.	n.d.	tr. ph	n.d.	86	n.a.	n.a.
KR5 as.3	banded?	2	76.2	10.8	13.0	n.d.	336000	180000	51000	5000	n.a.	n.a.	n.a.	tr. ph.	tr. ph	n.d.	919	n.a.	n.a.
KR5 as.4	banded?	1	86.4	8.3	5.2	n.d.	381000	44000	21000	15000	n.a.	n.a.	n.a.	tr. ph.	17700	107.8	12	n.a.	n.a.

Table DR1 (continued):

Salt melt inclusions with vapor bubble

Sample and assemblage	Qtz type	Total of inclusions	$FeCl_2$ (wt%)	KCl (wt%)	NaCl (wt%)	Cl (ppm)	Fe (ppm)	K (ppm)	Na (ppm)	Mg (ppm)	Pb (ppm)	Ca (ppm)	Mn (ppm))	S* (ppm)	Cu* (ppm)	Au* (ppm)	Ag* (ppm)	Cs (ppm)	Al (ppm)
DVE4_140.3 as.1	A?	2	41.3	36.5	22.2	470000	182000	192000	87000	n.a.	n.a.	n.a.	n.a.	17300	190	18.8	314	n.a.	n.a.
DVE4_140.3 as.2	A	6	48.6	35.2	15.4	492000	214000	184000	61000	300	n.a.	n.a.	n.a.	1500	360	4.8	119	n.a.	n.a.
DVE4_188.6 as.1	A	1	52.5	35.3	9.5	392000	231000	185000	37000	8000	n.a.	n.a.	n.a.	6600	2000	20.9	225	n.a.	n.a.
DVE4_188.6 as.2	A	10	52.3	37.8	9.4	446000	230000	198000	37000	3000	n.a.	n.a.	n.a.	4900	570	2.7	214	n.a.	n.a.
DVE5a_304.2 as.1	A?	4	50.8	24.4	21.1	415000	224000	128000	83000	52000	n.a.	n.a.	n.a.	800	30	3.5	n.a.	n.a.	n.a.
DVE5a_304.2 as.2	A?	2	57.4	25.7	17.0	242000	253000	135000	67000	115000	n.a.	n.a.	n.a.	8200	1000	10.2	n.a.	n.a.	n.a.
DVE5a_304.2 as.3	A	2	62.5	26.2	11.4	333000	275000	137000	45000	62000	n.a.	n.a.	n.a.	200	tr. ph.	2.0	107.1	n.a.	n.a.
DVE5a_304.2 as.4	A?	3	44.9	33.0	23.9	480000	198000	173000	94000	12000	n.a.	n.a.	n.a.	5400	230	8.5	48	n.a.	n.a.
DVE5a_369.6 as.1	A	11	49.6	33.2	15.2	514000	219000	174000	60000	1000	n.a.	n.a.	n.a.	9700	170	1.9	37	n.a.	n.a.
DVE5a_540.5 as.1	A or qtz xenolith	11	52.8	30.7	17.4	743000	233000	161000	68000	200	n.a.	n.a.	n.a.	3500	200	1.7	n.a.	n.a.	n.a.
DVE5a_104.6 as.1	qtz xenolith	5	40.6	32.3	22.7	561000	179000	169000	89000	300	n.a.	n.a.	n.a.	2200	9750	1.1	54	n.a.	n.a.
DVE5a_104.6 as.2	qtz xenotlith	7	59.1	27.3	13.4	463000	260000	143000	53000	n.a.	2500	9500	7500	600	8140	1.7	n.a.	111	59
DVE5a_104.6 as.3	qtz xenotlith	10	52.3	29.7	16.0	392000	231000	156000	63000	200	n.a.	n.a.	n.a.	3200	9010	0.9	117	n.a.	n.a.
DVE5a_104.6 as.4	qtz xenotlith	3	50.9	37.8	18.9	755000	224000	198000	74000	n.a.	n.a.	n.a.	n.a.	4400	7140	0.4	110	n.a.	n.a.
DVE5a_104.6 as.5	qtz xenotlith	2	58.8	29.3	11.9	525000	259000	154000	47000	n.a.	n.a.	n.a.	n.a.	7200	9500	1.1	n.a.	n.a.	n.a.
DVE5a_104.6 as.6	qtz xenotlith	4	44.9	32.5	22.9	649000	198000	170000	90000	n.a.	n.a.	n.a.	n.a.	54001	7620	1.5	120	n.a.	n.a.
DVE5a_104.6 as.7	qtz xenotlith	1	61.9	17.8	20.3	158000	273000	93000	80000	2000	n.a.	n.a.	n.a.	tr. ph.	tr. ph.	43.2	tr. ph.	n.a.	n.a.
DVE5a_104.6 as.8	qtz xenotlith	2	48.4	29.3	22.3	573000	213000	153000	88000	7000	n.a.	n.a.	n.a.	8000	11180	4.6	59	n.a.	n.a.

Vapor-free salt melt inclusions

Sample and assemblage	Qtz type	Total of inclusions	$FeCl_2$ (wt%)	KCl (wt%)	NaCl (wt%)	Cl (ppm)	Fe (ppm)	K (ppm)	Na (ppm)	Mg (ppm)	Pb (ppm)	Ca (ppm)	Mn (ppm))	S* (ppm)	Cu* (ppm)	Au* (ppm)	Ag* (ppm)	Cs (ppm)	Al (ppm)
DVE4_140.3 as.1	?	2	53.8	33.1	13.1	1115000	237000	174000	51000	n.d.	n.a.	n.a.	n.a.	60900	360	3.5	n.a.	n.a.	n.a.
DVE5a_369.6 as.1	A	2	47.7	33.4	18.9	738000	210000	175000	74000	n.a.	n.a.	n.a.	n.a.	14800	750	3.5	n.a.	n.a.	n.a.
DVE5a_369.6 as.3	banded	2	49.0	9.3	41.7	1726000	216000	49000	164000	n.a.	n.a.	n.a.	n.a.	42700	680	4.6	n.a.	n.a.	n.a.
DVE5a_540.5 as.1	A or earlier	2	65.3	24.8	9.9	337000	288000	52000	98000	152000	n.a.	n.a.	n.a.	2500	1900	1.1	n.a.	n.a.	n.a.
DVE5a_540.5 as.2	A or earlier	9	43.5	26.2	27.3	743000	192000	138000	107000	18000	n.a.	n.a.	n.a.	12100	260	2.9	n.a.	n.a.	n.a.
DVE5a_104.6 as.1	qtz xenotlith	4	37.9	36.5	23.7	n.a.	167000	191000	93000	n.a.	n.a.	n.a.	n.a.	66300	tr. ph.	8.1	n.a.	n.a.	n.a.

Analyses performed at the Department of Earth Sciences at ETH Zürich (ETH-GeoLas 193 nm Excimer Laser system, Elan 6100 quadrupole ICPMS; Günther et al. 1998; Heinrich et al., 2003), with quantification of analytical signals using the program SILLS (Guillong et al., 2008). Inclusions were studied in 6 core samples, representing quartz veining from different depths (104 to 540 m along drill holes, i.e. 85 to 443 m below surface). Samples DVE-5a/104.7; DVE-5a/540.5 contain small quartz aggregates (vein xenoliths) entrapped in porphyry. Table shows mean concentrations in individual fluid inclusion assemblages, sorted according to three inclusion types (vapor inclusions with no visible salt; salt melt inclusions with and without vapor bubble). S*, Cu*, Au*, Ag* columns include averages of detected values as well as individual limits of detection, to avoid the bias resulting from averaging only the highest values in a population with significant variations close to the limit of detection. S values are uncertain and may represent sulfate or minor sulfide. For all other elements only data clearly above limit of detection (LOD) were used. A few outlier analyses with highly inconsistent concentration of normalized major elements within an assemblages, and individual, very high concentrations of Mg, Cu or S apparently related to entrapment of solid phases into inclusions (separate element peaks not correlating with major elements) were excluded. Cl was analysed but its low signals yield much greater scatter than that of major cation ratios. Therefore, chloride concentrations were calculated based on assumption that the sum of major salts is 100% ($NaCl+KCl+FeCl_2$ = 100%). For vapor inclusions, the same normalization to 100% salt ignores the unknown proportion of water and reflects the likelyhood that these LA-ICPMS signals are dominated by co-entrapment of some salt melt with the low-density hydrous vapor. Cu and Au grades from 1 m long section of core that included the studied samples (data provided by EMED Mining, values in ppm) are: DVE4/140.3: 0.84 Au, 210 Cu; DVE4/188.6: 1.36 Au, 564 Cu; DVE5a/304.2: 0.23 Au, 77 Cu; DVE5a/369.6 : 0.8 Au, 774 Cu; DVE5/104.6: 0.1 Au, 65 Cu

A = A-type veinlet (based on terminology of Gustafson and Hunt, 1975), n.a. = not analysed, n.d. = not detected, tr. ph. = contains trapped phase with the analysed element

APPENDIX DR2: Supplementary analyses, photomicrographs and comparative data compilation

Micro-Raman data showing that salt melt inclusions are largely water-free

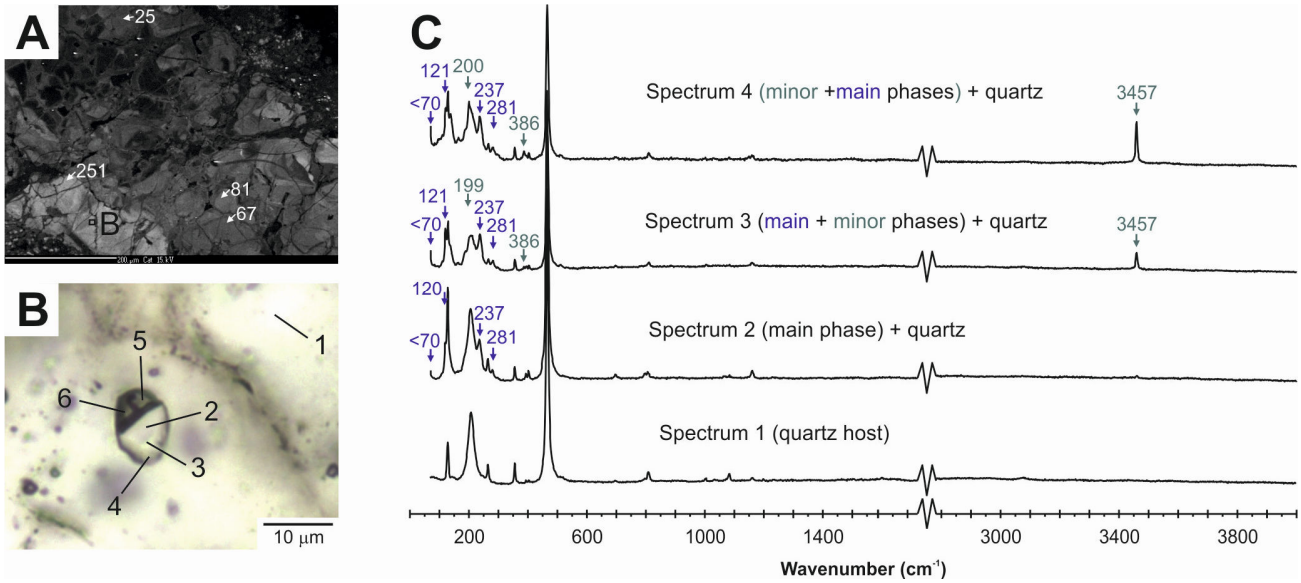

Figure DR1: Example of typical Laser Raman spectra of a salt melt inclusion in quartz veinlet from the Biely Vrch porphyry gold deposit, consisting of at least two solid phases, a distorted vapor bubble but no liquid at room temperature (sample DVE-4/112.4). A. SEM-CL image of the quartz veinlet hosting the inclusion in B, with arrows pointing to spots where Ti content was analysed (in ppm). B. Photomicrograph of the salt melt inclusion, with lines showing individual points analysed by Raman microprobe. C. Raman spectra of solid phases inside the inclusion and the host quartz. Raman peaks of the main mass of the inclusion are labelled in blue color and probably correspond to $FeCl_2$ and/or K_2FeCl_3 (based on phase relations in the NaCl-KCl-$FeCl_2$ molten salt system; see text and Fig. 5B). Green labels point to peaks ascribed to an unknown minor solid phase that frequently occurs in salt melt inclusions at Biely Vrch. Its sharp and strong peak at ~3457 cm^{-1} probably corresponds to OH stretching band typical for minerals containing hydroxyl groups. The same Raman peaks were observed in brine inclusions in several other porphyry systems (Kodăr et al., 2003, 2010), but the corresponding mineral composition is not known yet. Analyses in points 5 and 6 did not show any peaks except of the host quartz. Note, that none of the analyses show the presence of any liquid water nor water in salt hydrates, which would be evident from large overlapping bands in the OH stretching region of water at 2800 to 4000 cm^{-1} (Frezzotti et al., 2012).

Microthermometric observations on salt melt inclusions during heating

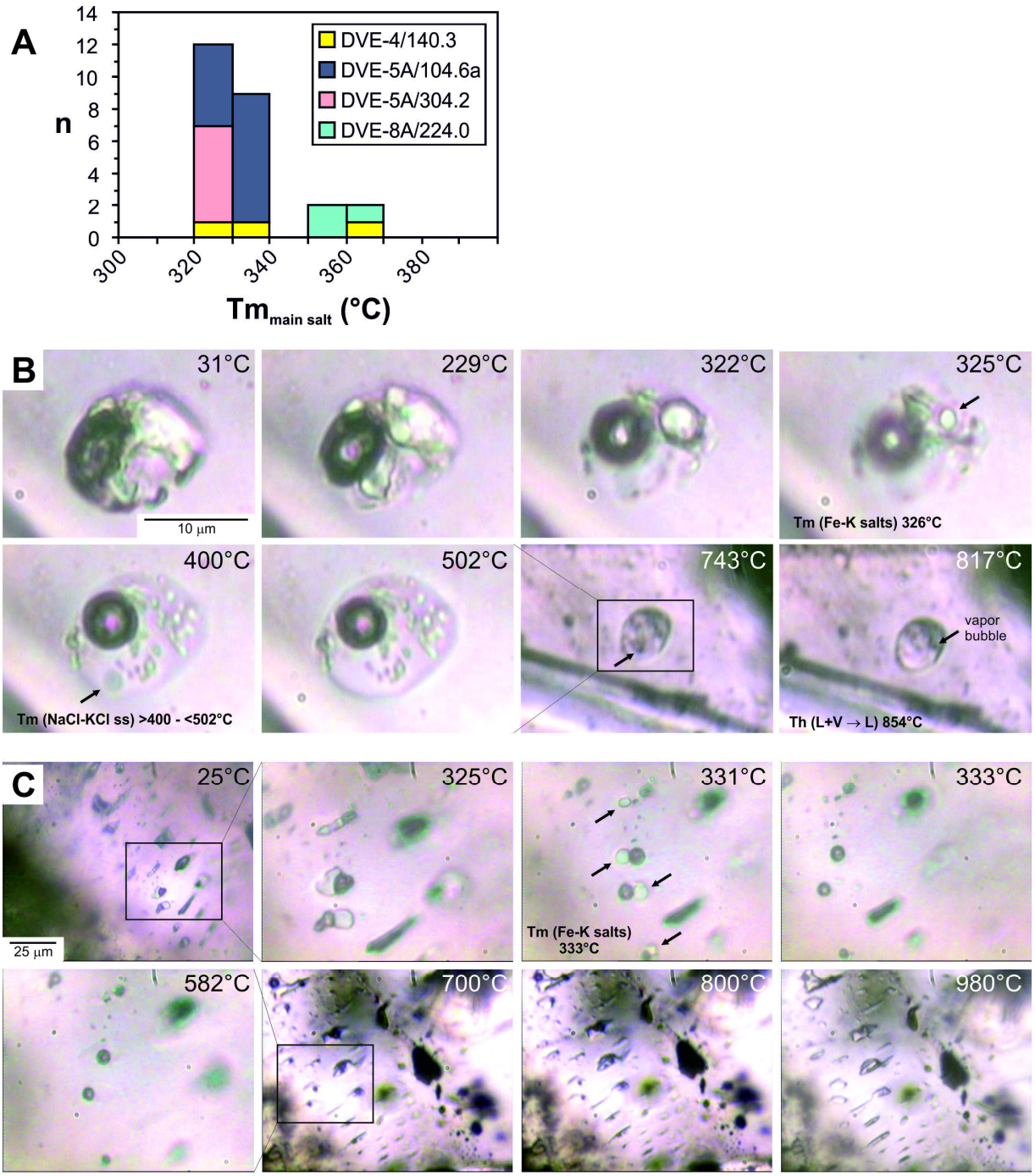

Figure DR2: Microthermometry data and appearance of salt melt inclusions during heating to specified temperatures, with arrows pointing to phases (daughter minerals and vapor) close to their disappearance. A. Frequency histogram of final melting temperature (Tm) of the main salts ($FeCl_2$ and/or K_2FeCl_3). B. Images of a typical large salt melt inclusion (sample DVE-5A/304.2). Quick dissolution of main salts at 326°C is followed by dissolution of a hardly visible solid, probably halite (>400°C; NaCl-KCl solid solution), but some other daughter minerals are still present in the inclusion. Liquid-vapor homogenization to liquid occurred at 854°C. C. Assemblage of salt melt inclusions in sample DVE-5A/104.6. Rapid dissolution of the dominant Fe-K salt crystal(s) occurred at 333°C, but halite dissolution was not observed. Note that most inclusions did not reach vapor-liquid homogenization up to 980°C, but keep consistent liquid-vapor ratios, indicating homogeneous entrapment but possibly some post-entrapment modification.

LA-ICPMS analyses differentiating samples and inclusion types (cf. Fig. 3 in paper)

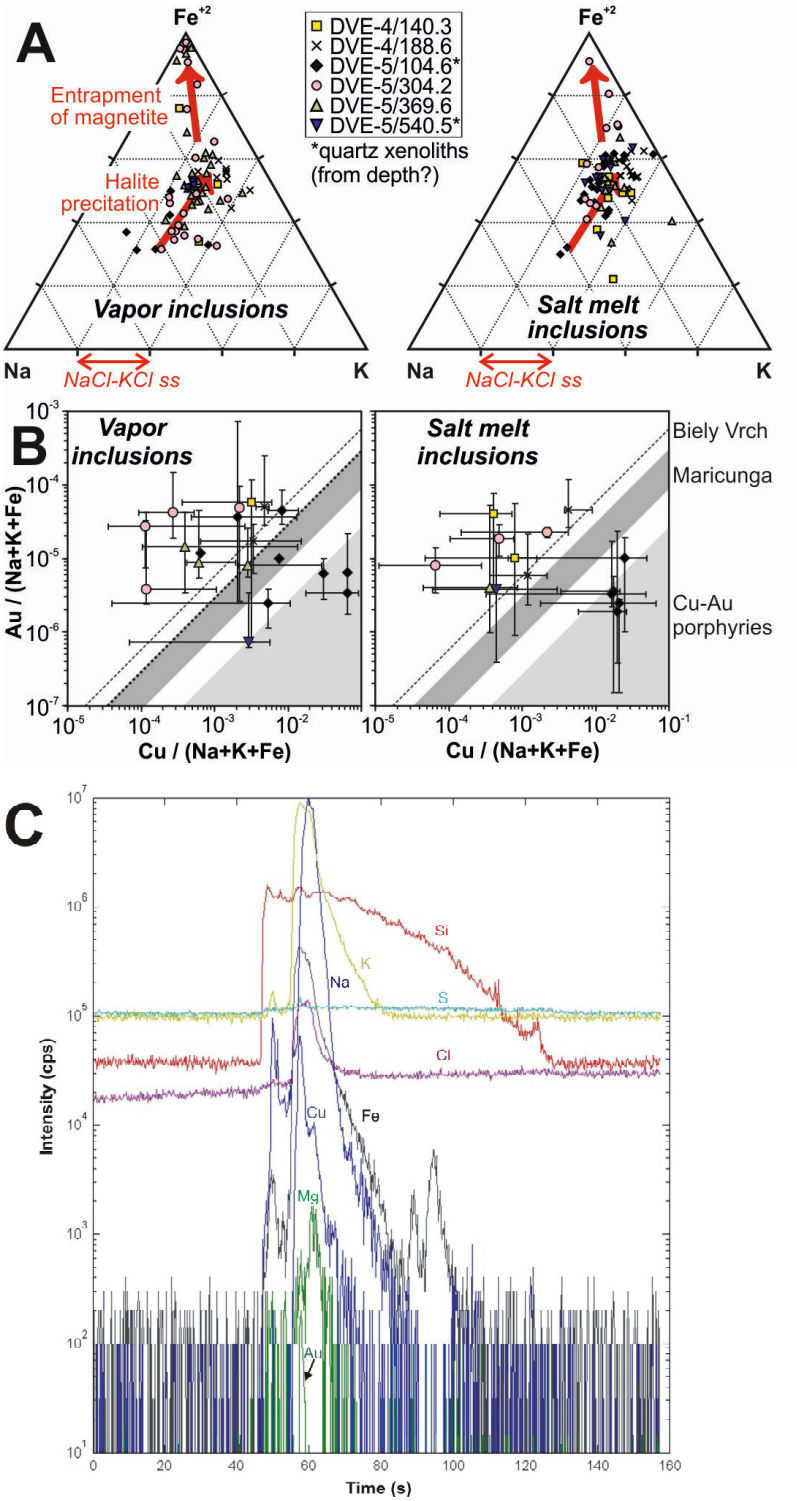

Figure DR3: LA-ICPMS microanalyses of fluid inclusions from the Biely Vrch deposit as measured in individual samples: A. Molar variation of major cations in individual inclusions with interpretation of major trends. B. Copper vs. gold concentrations based on mean values of individual inclusion assemblages. Diagonal bands show average Cu/Au ratios of ores at Biely Vrch, Maricunga Au-porphyries and at worldwide Cu-Au porphyries. C. Example of a transient LA-ICPMS signal obtained from a typical salt melt inclusion

Comparison of fluid compositions and metal ratios in magmatic-hydrothermal deposits

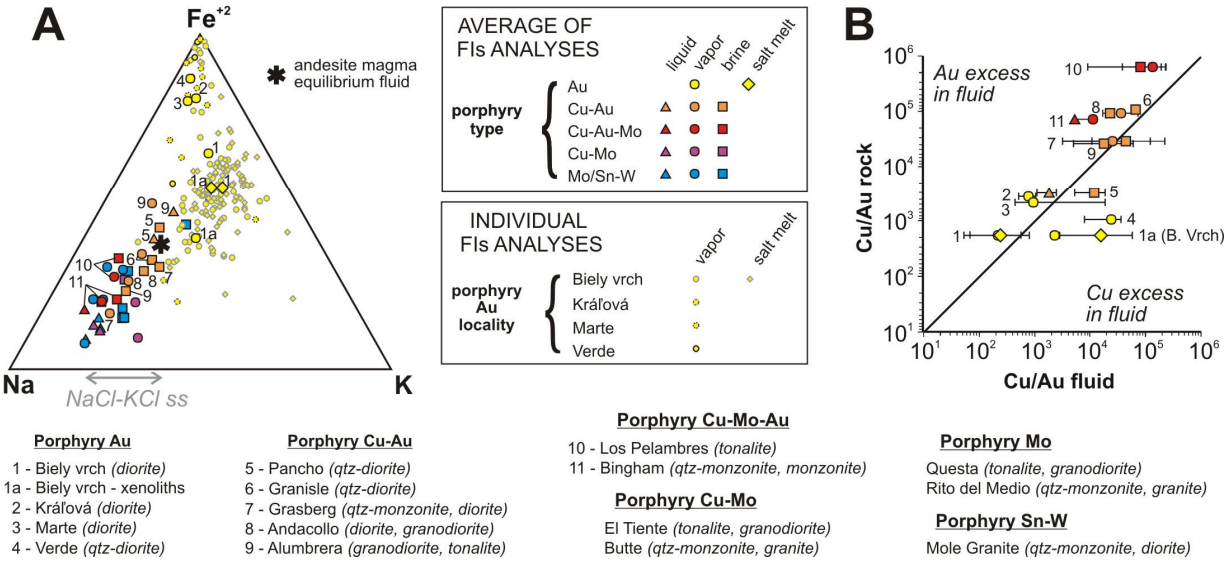

Figure DR4: Compilation on LA-ICPMS data from fluid inclusions in selected porphyry deposits (Klemm, 2005; Aillaud, 2010; this study). A. Average molar proportion of major cations with information on type of analysed inclusions, main commodities and composition of parental intrusives. Affiliation of porphyry Cu-Mo, Mo and Sn-W localities to data points has been omitted for clarity. Also shown is composition of volatile phase in equilibrium with andesite magma (Zajacz, 2012) and composition of individual fluid inclusions (FIs) from porphyry Au deposits. B. Comparison of molar Cu/Au ratios of bulk ore grades and corresponding mean values of fluid inclusions from Au-rich porphyry deposits.

ADDITIONAL REFERENCES CITED IN REPOSITORY CAPTIONS

Aillaud, B.J., 2010, Using fluid inclusions to trace formative fluid evolution at the Verde and Pancho porphyry Au deposits of the Refugio district, Chile [Ms.C. thesis]: Las Vegas, University of Nevada, 130 p.

Guillong, M., Meier, D.L., Allan, M.M., Heinrich, C.A., and Yardley, B.W.D., 2008, SILLS: A MATLAB-based program for the reduction of laser ablation ICP-MS data of homogeneous materials and inclusions: Mineralogical Association of Canada Short Course v. 40, p. 328-333.

Günther, D., Audétat, A., Frischknecht, R., Heinrich, C.A., 1998, Quantitative analysis of major, minor and trace elements in fluid inclusions using laser ablation inductively coupled plasma mass spectrometry: Journal of Analytical Atomic Spectrometry, v. 13, p. 263-270.

Heinrich, C.A., Pettke, T., Halter, W.E., Aigner-Torres, M., Audetat, A., Gunther, D., Hattendorf, B., Bleiner, D., Guillong, M., Horn, I., 2003, Quantitative multi-element analysis of minerals, fluid and melt inclusions by laser-ablation inductively-coupled-plasma mass-spectrometry: Geochimica et Cosmochimica Acta, v. 67, p. 3473-3497.

Frezzotti, M.L., Tecce, F., and Casagli, A., 2012, Raman spectroscopy for fluid inclusion analysis: Journal of Geochemical Exploration, v. 112, p. 1-20.

Koděra, P., Rankin, A.H., and Murphy, P.J., 2003, Identification of some Fe-bearing daughter minerals in fluid inclusions using Raman spectroscopy: *in* Abstracts of the XVII ECROFI conference: Acta Mineralogica Petrographica Abstract Series, v. 2, p. 101-102.

Koděra, P., Lexa, J., and Fallick, A.E., 2010, Formation of the Vysoká–Zlatno Cu–Au skarn–porphyry deposit, Slovakia: Mineralium Deposita, v. 45, p. 817-843.

Klemm, 2005, Cu-Mo-Au ratios in porphyry-type ore deposits: constraints from fluid inclusion microanalysis, Ph.D. Thesis 16395: Zürich, Swiss Federal Institute of Technology, 162 p.

Zajacz, Z., Candela P.A., Piccoli, P.M., and Sanchez-Valle, C., 2012, The partitioning of sulfur and chlorine between andesite melts and magmatic volatiles and the exchange coefficients of major cations: Geochimica et Cosmochimica Acta, v. 89, p. 81–101.